Large Ellipsoid Parts Manufacture Using Electromagnetic Incremental Forming With Variable Blankholder Structure

Xiaohui Cui (cuixh622@csu.edu.cn)
Central south University
Yan Ziqin
Central south University
Chen Baoguo
COMAC Shanghai Aircraft Manufacturing Co., Ltd., Shanghai
Du Zhihao
Central South University
Xiao Ang
Central South University
Yu Hailiang
Central south University

Research Article

Keywords: Large ellipsoid parts, Electromagnetic incremental forming, Variable blank holder structure, Wrinkle, Numerical simulation

Posted Date: March 18th, 2021

DOI: https://doi.org/10.21203/rs.3.rs-308311/v1

Version of Record: A version of this preprint was published at The International Journal of Advanced Manufacturing Technology on July 22nd, 2021. See the published version at https://doi.org/10.1007/s00170-021-07695-y.

Abstract

The large ellipsoid parts are the main load-bearing components in the rocket tank, which are prone to wrinkle when using the traditional stamping. In order to solve the wrinkling problem in large parts, the EMIF method with a variable blank holder is proposed in this paper. The numerical simulation has shown that the sheet material near the blank holder is, as a consequence of stamping, subjected to circumferential compressive stress. When the drawing height was 100 mm, the sheet metal was notably wrinkled. In the electromagnetic forming (EMF) process, the sheet region facing the coil becomes thinner. However, the sheet metal thickness corresponding to the coil edge increases with the increase in forming height. If the EMF forming height is 150 mm, the sheet, which is in contact with the smooth mold, is deformed without a wrinkle. Compared to the traditional stamping, the EMF can significantly reduce the sheet metal wrinkling, improving the deformation height of the sheet metal smooth area.

1. Introduction

With the increasing demand for high-speed trains, large aircraft, and large carrier rockets requiring integral, high-precision, and lightweight structural parts, the sheet parts are developing rapidly. There is a need for producing the parts of larger size, thinner walls, deeper cavities, and more complex surfaces, all while using difficult-to-deform materials. The application of high-performance lightweight alloys for manufacturing large integral components is the primary technical direction for increasing the part bearing capacity limit in both the aviation and aerospace. For example, the aluminum alloy has several advantages, including the low density, high strength, and corrosion resistance; as such, it has been widely used in the aerospace field.

Large-scale ellipsoid parts are the key components of rocket tank; the desired shape is mainly achieved by applying the mechanical force and liquid pressure to drive part deformation. Currently, there are two main methods for manufacturing the large rocket tank: (1) decomposing the part into smaller parts, which are then welded together after forming or (2) using heavy equipment to achieve the integral manufacturing of large parts.

For the former (1), there are several examples. Feng et al. [1] designed a melon petal dies through numerical simulation and experimental research; the results were then applied to successfully manufacture the smooth surface and wrinkle-free melon flap parts (the deep drawing was used). However, the drawing forming needs multiple mold tests, increasing the mold manufacturing cost. Yang et al. [2] found pre-deformation introduced in creep age forming can reduce springback and improve mechanical performances. Xu et al. [3] found the creep deformation is improved and the springback is reduced in the non-isothermal creep ageing process, in compared with the isothermal creep ageing process. Yang et al. [4] established the finite element model of creep aging forming to manufacture the vehicle fuel tank melon flap. By analyzing the creep strain, equivalent stress, and yield strength, the melon flap parts of a carrier rocket fuel tank were successfully manufactured. However, the creep aging forming has several limitations, including the long production cycle and high cost - both the forming molds and

hot pressing tanks are expensive. Additionally, the accurate springback prediction is another problem encountered when using creep aging [5–6]. For this reason, the traditional rocket tank manufacturing process by using melon petal forming and welding generally has low manufacturing efficiency and poor performance.

Regarding the latter, the use of heavy equipment to produce the large parts (2), China's largest vertical spinning machine with (1000 kN capacity) has the following dimensions: it is 30 m long, 18 m wide, and stands 13 m tall [7]. However, it can process the parts with maximum diameter up to 2 m. Similarly, Yuan et al. [8] have built the double-acting sheet metal hydraulic forming equipment with the world's largest tonnage – 150 MN. The machine is 19.5 m high and has a 4.5 m × 4.5 m working table. It is evident that the huge structure and high price inherent to large equipment pose a great challenge to the equipment manufacturing industry. Therefore, enabling the use of smaller equipment to precisely manufacture the large, thin-walled, and curved aluminum alloy parts is among the critical scientific and technological problems.

The electromagnetic forming (EMF) is a type of special processing method with both high energy rate and high speed. Compared with the traditional quasi-static forming method, EMF technology has a higher speed and the advantage of being non-contact method. This allowed it to greatly improve the material forming limit, simplify the mold manufacturing, reduce residual stress, enhance forming accuracy, and easily control the energy, improving the production automation. For example, Cui et al. [9–10] simulated the electromagnetically-assisted forming of V-shaped and U-shaped parts. Cui et al. [11] proposed a novel reverse-bending method using EMF. The plastic-strain increases and stress decreases were found in the sheet-bending region following the electromagnetic forming. It should be noted that all the studies presented above show that EMF substantially reduces the springback.

Currently, there are two main strategies for manufacturing the large size parts using EMF:

1. Using high-energy equipment and a large coil structure – Lai et al. [12] established an electromagnetic forming device without the assistance of traditional stamping. Combined with the electromagnetic blanking and inertial constraints, 5083-O aluminum alloy hemisphere part with about 1000 mm diameter and 225 mm deep was successfully developed. However, two sets of electromagnetic forming devices over 800 kJ discharge energy and thecoil diameters over 800 mm were required.
2. A low-energy equipment and a small coil structure – adopted to achieve the integral forming by moving the coil discharge. Cui et al. [13] proposed electromagnetic incremental forming (EMIF). In this method, the working coil moves step-by-step along the mold profile, with each step being discharged twice in each position. The first discharge reduces the distance between the sheet and the mold profile, while the second one makes the sheet and mold fit completely.

Tan et al. [14] used EMIF to successfully develop a double-curvature integral wainboard. The influence of technological parameters such as discharge voltage, capacitance, coil height, discharge path, and coil

and mold fit overlap ratio was studied experimentally. Furthermore, Li et al. [15] analyzed the forming mechanism and defect law in large-sized curved surfaces made of aluminum alloy using the EMIF process. They used numerical simulation and experimental verification, finding that the wrinkling was primarily caused by the circumferential compressive stress, which was a consequence of stress wave propagation caused by electric discharge. Finally, Cui et al. [16] proposed the electromagnetic partitioning forming to achieve precise manufacturing and control the springback when producing curved parts.

Cui et al. [17] combined the traditional drawing process and the EMIF aiming to manufacture large curved thin-walled parts made of aluminum alloy. After 36 discharges, curved surface parts with a 580 mm diameter and a height of nearly 75 mm were obtained. When the blank holder radius is set to 390 mm, the deformed sheet surface is smooth, and there are no wrinkles, as shown in Fig. 1(a). Inside the dotted red line, the sheet regions deformed using die are shown. Furthermore, to obtain a larger ellipsoid part, the blank holder radius is enlarged to 475 mm. When the forming height is 60 mm, the notable wrinkles appear on the sheet surface (see Fig. 1(b)); therefore, the wrinkling problem must be solved when forming large parts.

In this paper, we applied the electromagnetic incremental forming with a variable blank holder structure, aiming to manufacture larger parts. The thickness-to-diameter ratio of sheet metal is approximately 0.1%, which causes severe wrinkling on sheet in traditional drawing processes. The numerical simulation and the experiment were carried out to analyze the forming process and wrinkling in large parts, both in traditional drawing and EMIF process.

2. Forming Principle

Figure 2 shows the EMIF process using variable blank holder structure. The forming system includes the forming die, pressing plate, support plate, working coil, sheet, and hydro-cylinder. The pressing plate and supporting plate are used to press the sheet metal, which is then deformed in deep drawing direction under the action of hydro-cylinder and magnetic force.

The whole forming principle is carried out in two steps:

1. For the blank holder radius R_1, the part is formed in steps with the final forming depth being the H_1.
2. The blank holder radius size is changed to R_2, and the part is formed in steps. The final forming depth is set to H_2.

3. Quasi-static Forming

3.1. Wrinkle simulation

The quasi-static forming process is shown in Fig. 3. The sheet made of 3003-O aluminum alloy and its diameter is 1150 mm with 1 mm thickness. The material yield strength and elastic modulus are 50 MPa and 68 GPa, respectively. The stress-strain relationship of the material properties was determined by

carrying out a uniaxial tensile experiment, as shown in Eq. (1). To consider how does the high strain rate affects the EMF process, the material behavior was modeled using the Cowper-Symonds power law, as shown in Eq. (2). The data used in Eq. 1 and Eq. 2 are taken from the paper published by [17].

$$\sigma_{qs} = 138(\varepsilon^{pl} + 0.0006)^{0.137} \quad (1)$$

$$\sigma = \sigma_{qs}\left(1 + \left(\frac{\dot{\varepsilon}^{pl}}{C_m}\right)^{\frac{1}{n}}\right) \quad (2)$$

where σ is the dynamic flow stress, σ_{qs} is the quasi-static flow stress, $\dot{\varepsilon}^{pl}$ is the strain rate, and C_m = 6500 s^{-1} and n = 4 are specific aluminum alloy parameters.

Figure 3(a) shows the forming system; the blank holder radius R is set to 475 mm, and the distance between the pressing plate and supporting plate is 2 mm. In this paper, the sheet metal thickness-to-diameter ratio is approximately 0.1%. The obvious sheet metal wrinkles will occur if the flange is not clamped by the pressing and supporting plates.

Figure 3(c) and Fig. 3(d) show the deformation results for the drawing depth of 100 mm. In Fig. 3(c), the C3D8 elements were used for sheet metal (a solid unit). On the other hand, in Fig. 3(d), the S4 sheet metal element type was used, which represents a shell unit. During the drawing process, the pressing plate, supporting plate, and punch were set as rigid bodies. The friction coefficient used within the study is set to 0.2. It is evident that the wrinkling will not occur on sheet metal when using solid elements. However, severe wrinkling appears on sheet metal when using shell elements, mainly since the large solid element stiffness is difficult to distort, yielding the incorrect wrinkling analysis simulation results. For these reasons, the shell element was used for the following considerations.

3.2 Single blank holder forming system (R = 475 mm)

Figure 4 shows the deformation results using a single blank holder forming system. The radius of the blank holder is 475 mm. The distance between the pressing plate and supporting plate is set to 1 mm, with the pressing force of 50000 N. The remaining simulation parameters are consistent with the Fig. 3 (d). Additionally, Fig. 4(a) shows that obvious wrinkle will appear on the sheet when the drawing depth is set to 100 mm.

To further analyze the wrinkling height, Path 1 was defined on the sheet; Fig. 4 (b) shows the displacement forming along the Path 1 direction. It is evident that the sheet metal deflection has noticeable waves. The maximum displacement is 92.3 mm, while the minimum displacement is 86 mm. Aiming to further analyze the sheet wrinkling cause, the element 5296 (near the blank holder) and element 3506 (near the sheet metal top) were selected. For the drawing depth of 100 mm, based on Fig. 4(c) and (d) it can be concluded that:

1. The radial (σ_r) and circumferential stress (σ_θ) of the element 3605 are 89.7 MPa and 83.5 MPa, respectively, meaning that the element is subjected to both radial and circumferential tensile stresses. Furthermore, its radial strain (ε_r), circumferential strain (ε_θ), and thickness strain (ε_t) are 0.0213, 0.0122, and − 0.0335, respectively. Based on the presented values, it can be concluded that the element 3605 appears to be thinning (reducing in thickness).
2. The radial and circumferential element 5296 stresses are 17 MPa and − 71.7 MPa, respectively. Its radial, circumferential, and thickness strain are 0.013, -0.021, and 0.008, respectively. Finally, the element 5296 thickness increases, causing wrinkles in the region near the blank holder.

Node 9597 on element 5296 and node 7765 on element 3605 were extracted, and the stress and strain variation trends are shown in Fig. 5. The node 7765 is subjected to both radial and circumferential tensile stresses and strains; the tensile stress and strain increase with the increase in forming height, leading to the decrease in stress and strain thickness as the drawing height increases. If the forming height is between 0 and 17 mm, the node 9597 is acted upon by a low radial tensile stress, while the circumferential stress is practically 0. If the forming height is between 17 and 100 mm, the circumferential compressive stress measured in node 9597 gradually increases. Furthermore, the circumferential compressive stress is much greater than the radial tensile stress, causing an increase in the thickness strain as the drawing height increases.

3.2. Two blank holder forming systems (R_1 = 390 mm, R_2 = 475 mm)

Aiming to reduce the sheet metal wrinkling, the forming method using a variable blank holder was proposed. Two blank holder radii were adopted: R_1 = 390 mm and R_2 = 475 mm, with a total drawing height of 100 mm. Finally, three forming schemes were created by adjusting the drawing height, as shown in Table 1.

Table.1 Forming schemes

	First blank holder (R_1 = 390 mm)	Second blank holder (R_2 = 475 mm)
Scheme 1	Forming height (H_1 = 50 mm)	Forming height (H_2 = 100 mm)
Scheme 2	Forming height (H_1 = 60 mm)	Forming height (H_2 = 100 mm)
Scheme 3	Forming height (H_1 = 70 mm)	Forming height (H_2 = 100 mm)

Figure 6 shows the stress distribution for various blank holder combinations. Figures 6 (a), (c), and (e) illustrate the stress distribution for drawing depths of 50 mm, 60 mm, and 70 mm while using the first blank holder (390 mm radius). In that case, the element 3897 (near the first blank holder) is subjected to radial tension stress and circumferential compressive stress. With the increase in the forming height, the radial tensile stress decreases while the circumferential compressive stress increases. Figures 6 (b), (d), and (f) show the stress distribution when the total forming height was 100 mm for all the three schemes.

Element 5296 (near the second blank holder) was subjected to greater circumferential compressive stress compared to element 3897. As a result, all three forming schemes with the variable blanking structure caused the noticeable wrinkling on the sheet metal (for the forming height of 100 mm).

In order to further analyze the cause behind the sheet metal wrinkling, Scheme 2 simulation results were selected. Figure 7 shows the changes in node 9597 stress and strain as time progresses. When the first block holder is used (R_1 = 390 mm), node 9597 is subjected to radial tensile stress and circumferential compressive stress. That corresponds to the radial tensile strain, circumferential compressive strains, and thickness tensile strains. The thickness strain increases sparsely and has a value of 0.057%. Furthermore, when the second blank holder (R_2 = 475 mm) is used, the node 9597 circumferential compressive strain increases significantly, causing the final thickness strain to increase sharply. Its value is 0.58%, given that the forming depth is 100 mm.

Figure 8 shows the final sheet deformation result and the change in the Path 1 displacement when using Scheme 2. The apparent wrinkling can be observed on the sheet, along with the displacement on Path 1, which also has obvious height variations. Such observations show that sheet material thickness strain has only increased by 0.58%; however, the sheet material has also displayed the obvious wrinkling behavior.

4. Electromagnetic Forming

4.1. Finite element model

Figure 9 (a) shows the electromagnetic field model established using ANSYS/EMAG software. The electromagnetic field model includes the far-field air, near-field air, coils, and sheets. Solid97 element type was used to model the near-field air, coil, and sheet metal, while the Inf111 element type was used for far-field air. Two spiral waist-shaped coils were symmetrically distributed on the sheet metal. For example, the deformed sheet and the coil position was shown in the 19th discharge (see Fig. 9 (b)). Regarding the current flow through the coil, it is well explained in the literature [17]. Following the coil discharge, Fig. 9(c) shows the electromagnetic force distribution across the sheet metal. Figure 9(d) shows the sheet forming system established using ABAQUS/EXPLICIT software; the sheet using the shell elements deforms along the Z-axis under the electromagnetic force action.

In order to solve the wrinkling sheet metal phenomenon in the large blank holders, as shown in Fig. 1 (b), the EMIF process with variable blank holder (Fig. 2) was adopted. The schematic diagram of the ensuing forming process is displayed in Fig. 10(a). In the each layer, the whole sheet was drawn for 15 mm. The coil discharges N times in this layer to ensure that the sheet and the die are in contact. The coil is required to rotate twice and discharge in each layer, primarily to ensure the sheet metal deformation uniformity. Furthermore, it is assumed that the distance between the inner coil wall and the sheet metal center is L (in the *n*-th layer). Figure 10(b) shows the discharge positions of the first turn; the angle between the coil

discharge position 2 and the horizontal sheet metal centerline is marked as α. During the second turn, the discharge positions were rotated for 0.5α in the counter-clockwise direction, as shown in Fig. 10(c).

In this paper, the forming process is carried out as follows: (1) the first blank holder radius R_1 is set to 390 mm and the forming height H_1 is 75 mm. (2) the second blank holder radius R_2 is set to 475 mm and the forming height H_1 is 150 mm. If both blank holders are used, the coil discharges in ten layers to ensure that the sheet is deformed in a step-by-step manner. The forming height H, distance L, rotation angle α, and the number of discharges N are shown in Table 2 and Table 3 for each layer.

Table.2 Discharge parameters using the first blank holder (R_1 = 390 mm)

	1st layer	2nd layer	3rd layer	4th layer	5th layer
H	15 mm	30 mm	45 mm	60 mm	75 mm
L	100 mm	160 mm	210 mm	250 mm	280 mm
α	90°	60°	45°	45°	30°
N	4	6	8	8	10

Table.3 Discharge parameters using the second blank holder (R_2 = 475 mm)

	6st layer	7nd layer	8rd layer	9th layer	10th layer
H	90 mm	105 mm	120 mm	135 mm	150 mm
L	295 mm	320 mm	345 mm	358 mm	370 mm
α	30°	30°	30°	30°	30°
N	10	10	10	10	10

4.2. The first blank holder forming system (L_1 = 780 mm, H_1 = 75 mm)

According to Table 2, forming data and the process presented in Fig. 10, the final sheet metal deformation shape in 2nd to 5th layers is shown in Fig. 11. Furthermore, the 10th, 18^h, 26th, and 36th coil discharge correspond to the last coil discharge in 2nd, 3rd, 4th, and 5th layer, respectively. Nodes 6370 and Node 8960 are located near the first blank holder edge; the displacement difference between said nodes is below 1 mm between 2nd and 5th layer. Thus, the overall sheet metal deformation is uniform – the sheet surface is smooth, and there are no noticeable wrinkles.

Aiming to fund why the sheet did not wrinkle when using the first blank holder, it is necessary to analyze the stress-strain and sheet thickness variation during the drawing and discharging processes. Figure 15 (a) shows the deformation profiles after the 26th discharge and 5th drawing. Moreover, Fig. 15 (b) shows

the sheet metal stress distribution after the 5th drawing. Element 3901, located near the blank holder, is subjected to both radial and circumferential compressive stresses, which potentially cause an increase in the sheet metal thickness strain. Figure 15(c) shows the increments of three principal strains at the Node 7778 during the 5th drawing process. Since the radial compressive stress is greater than its circumferential counterpart, the circumferential compressive sheet metal strain increments are smaller. Lastly, Fig. 15(d) shows the Node 7778 thickness increments in the 5th drawing process.

After the 5th drawing is carried out, the deformation results after the 27th coil discharge are shown in Fig. 16. Deformations of sheet metal parts facing the coil are evident. Nodes 6369 and 8970, corresponding to the coil middle and edge, are selected. Moreover, during the 27th coil discharge, the Node 6369 reduction in thickness becomes apparent, while the Node 8970 thickness slightly increases.

Figure 14 shows the changes in stress and strain distribution at nodes 6369 and 8970 depending on the time. The Node 6369 was subjected to radial and circumferential tensile stresses at 150 μs, after which the stress oscillated and, finally, decreased. The plastic strain increment at the Node 6369 during the 27th discharge is a radial tensile strain, circumferential tensile strain, and thickness compressive strain.

The Node 8970 was subjected to bi-directional compressive stress at 150 μs. The final strain increment is divided into radial and circumferential compressive strain and thickness tensile strain. This results in a slight increase in the sheet metal thickness corresponding to the coil edge (as shown in Fig. 13). However, the sheet metal does not wrinkle during the 5th drawing process due to a very small increase in the circumferential compressive strain (see Figs. 13 and 14).

4.3. The second blank holder forming system (R_2 = 475 mm, H_2 = 150 mm)

Using the forming data provided in Table 3, the final deformed shapes for the layers 6 to 9 are shown in Fig. 18. The 46th, 56th, 66th, and 76th coil discharge correspond to the final coil discharges in 6th, 7th, 8th, and 9th layer. It can be seen that the deformed sheet surface is smooth, with no discernable wrinkles.

Nodes 9953 and 9957 located near the edge of the second blank holder (R_2 = 475 mm) are selected next. The displacement difference between the nodes is approximately 3 mm in the 9th layer. Furthermore, the sheet region deformations near the second blank holder become inhomogeneous as the forming depth increases; therefore, a minor wrinkle could take place at the sheet region near the blank holder.

Assuming that the second blank holder (R_2 = 475 mm) is used, variations in stress, strain, and thickness with time caused by the drawing and discharging processes are analyzed. The deformed sheet profiles following the 76th discharge and 10th drawing are shown in Fig. 16(a). Moreover, Fig. 16 (b) shows the stress distribution on the sheet after the 10th drawing; the element 5296 is subjected to bi-directional compressive stress.

After comparing Fig. 12 and Fig. 16, it is evident that, during the drawing process, the sheet region near the blank holder is subjected to bi-directional compressive stress. When the blank holder diameter increases, the circumferential compressive sheet metal strain increases. Figure 16(c) shows the changes in stress with time at the Node 9597 (during the 10th drawing). In the radial and circumferential directions, sheet metal is subjected to compressive stresses. Additionally, the thickness sheet metal strain should be increased.

Figure 16(d) shows the radial and circumferential compressive strains which have caused an increase in thickness strain. Furthermore, since the circumferential compressive strain has a significant role in the thickness increase, the wrinkling trend will also increase.

Following the 10th drawing, Fig. 18 shows the sheet deformation results after the 77th coil discharge. Nodes 9145 and 9954 were selected, corresponding to the coil middle and coil edge, respectively. Moreover, during the 77th EMF process, the Node 9145 thickness decreased significantly, while the Node 9954 thickness increased. After comparing Figs. 13 and 17, it is clear that, with the increase in the blank holder diameter, the thickness of the sheet region facing the coil edge increases significantly following the coil discharge.

Figure 18 shows the changes in stress and strain of nodes 9145 and 9954 as time progresses. At 120 μs, the Node 9145 is subjected to the bi-directional tensile stress, while the stress varies in the later stages. The Node 9145 strain increments during the discharge are as follows: radial and circumferential tensile strain and thickness compressive strain. It can be seen that Node 9145 thickness is reducing; therefore, the coil is in the position opposite to the plate during the discharge process, thus preventing the wrinkling.

The Node 9954 is subjected to bi-directional compressive stress at 150 μs. The final strain increment ratio of sheet metal is circumferential compressive strain and thickness tensile strain. Such strain arrangement eventually results in a slight increase in the sheet thickness located near the coil edge. Thus, based on the analysis above, it can be stated that:

1. The thickness deformation reduction mainly occurs in the position where the coil is facing the sheet; in that position, there will be no wrinkling;
2. The thickness of the coil edge area increases due to the circumferential compressive stress, which may cause wrinkling. Moreover, with the increase in the blank holder diameter, the coil edge area thickness increment increases.

Figure 19 shows the final deformation of the sheet after 10 times of drawing and 86 times of coil discharge. In Fig. 19(a), the sheet metal inside the white dotted line is uniformly deformed and has a smooth surface. Local pits and bulges have appeared on sheet material outside the white dotted line, which nears the blankholder. Compared with the drawing results in Fig. 8, the new method adopted in this paper can significantly reduce the wrinkling and avoid wrinkling into the deformed smooth area of sheet metal. Figure 19(b) shows the thickness distribution of sheet metal.

5. The Experiment

Figures 20 (a) and (b) show the drawing results obtained using different blank holders. The former, Fig. 20(a), shows the blank holder with the radius of 390 mm; in that case, the sheet metal surface is smooth and without wrinkles (assuming that the drawing height is 60 mm). Based on Fig. 20(a), Fig. 20(b) shows the sheet deformed using the 475 mm radius blank holder. The associated drawing height is 100 mm, and there is apparent wrinkling appearing on the sheet. In other words, the wrinkles appear on the previously smooth surface.

Figure 20(c) shows the process using 390 mm radius blank holder. The resulting sheet metal surface is smooth and without wrinkling when the forming height is 75 mm. Finally, Fig. 20(d) shows the deformation sheet metal when R_2 = 475 mm. The deformed sheet area located inside the red dotted line is smooth and without wrinkling, while the area surrounding the pressing edge displays a lower degree of wrinkling. Such behavior is mainly caused by the sheet metal corresponding to the coil edge, which will be thicker due to the action of circumferential compressive stress when discharging. Finally, it should also be added that the circumferential compressive strain increases with the increase in the blank holder size.

In this paper, the total discharging time is 86, while the drawing times are 10 for obtaining the final shape (shown in Fig. 20(d)). Finally, Fig. 21 shows the distribution of profile deformation and thickness in the experiment and the simulation. It is evident that both the sheet metal deformation profile and thickness distribution are in agreement with the experimental results. In the traditional single point incremental forming (IF), the material is difficult to flow. Thus, the sheet occurs thinning deformation, and the thickness of the sheet is calculated according to the sine theorem. In Fig. 21(b), the minimum thickness is 0.691, 0.91 and 0.89 mm for the IF process, the numerical simulations and the experimental data from 0 to 350 mm, respectively. Thus, the new method in this paper can inhibit thickness thinning.

6. Conclusions

1. The electromagnetic forming method supplemented with the use of variable blank holder is proposed to reduce the wrinkling in the manufacturing of large ellipsoid parts. The proposed simulation method was found to accurately predict the sheet forming process in both the quasi-static drawing and electromagnetic forming.
2. In the traditional drawing process, the sheet material near the blank holder is subjected to radial tensile stress and circumferential compressive stress. With the increase in forming height or when the blank holder is increased, the circumferential compressive strain near the blank holder rises. Finally, when the forming height is 100 mm, the sheet material wrinkling becomes apparent.
3. During the coil discharge, the sheet region facing the coil is subjected to both radial and circumferential tension strain. For this reason, the electromagnetic forming is helpful to reduce the wrinkling during the forming of large parts. However, with the increase in the blank holder diameter, the sheet metal region corresponding to the coil edge has a minuscule increase in thickness, causing

an increase in the wrinkling. Finally, when the forming height is 150 mm, the sheet material near the blank holder becomes wrinkled; however, the sheet region in contact with the dye has no wrinkling.

Declarations

Ethical Approval

Not applicable.

Consent to Participate

Written informed consent for publication was obtained from all participants.

Consent to Publish

Written informed consent for publication was obtained from all participants.

Authors Contributions

Xiaohui Cui: Methodology, Investigation, Simulation, Experiments, Writing - review &editing.

Ziqin Yan: Methodology, Investigation, Writing.

Baoguo Chen: Investigation.

Zhihao Du: Investigation, Collected data, Experiments.

Ang Xiao: Simulation, Collected data.

Hailiang Yu: Review &editing, Investigation.

Funding

This work was supported by the National Natural Science Foundation of China (Grant Number: 51775563 and 51405173), Innovation Driven Program of Central South University (Grant number: 2019CX006), the Project of State Key Laboratory of High Performance Complex Manufacturing, Central South University (ZZYJKT2020-02).

Competing Interests

The authors declare no conflict of interest

Availability of data and materials

All data and materials are fully available without restriction.

References

1. Feng, S.L., Li, L.C., Luo, Y.M., Shen, H.H., Xu, A.J., Yang, X.Q. Deep drawing technology for large diameter double curvature aluminum alloy thin-walled part. Aerospace Shanghai. 2019, 2: 104-110.
2. Yang, Y.L., Zhan, L.H., Ma, Q.Q., Feng, J.W., Li, X.M. 2016. Effect of pre-deformation on creep age forming of AA2219 plate: Springback, microstructures and mechanical properties. J. Mater. Process. Technol. 229: 697-702.
3. Xu, Q.Q., Zhan, L.H., Huang, M.H., Shen, R.L., Ma, Z.Y., Xu, L.Z., Wang, K., Wang, X. 2018. Deformation behavior of Al-Cu-Mg alloy during non-isothermal creep age forming process. J. Mater. Process. Technol. 255: 26-34.
4. Yang, Z., Zhan, L.H., Wang, M., Cahng, Z.L., Ma, Y.L., Wan, L. Simulation and experiment on creep aging for thin wall component with ellipsoid surface. Forging and stamping technology. 2018, 2: 76-83.
5. Lam, A., Shi, Z.S., Yang, H.L., Wan, L., Davies, C.M., Lin, J.G., Zhou, S.J. Creep-age forming AA2219 plates with different stiffener designs and pre-form age conditions: Experimental and finite element studies. J. Mater. Process. Technol. 2015, 219: 155-163.
6. Guines, D., Gavrus, A., Ragneau, E. Numerical modeling of integrally stiffened structures forming from creep age forming technique. Int J Mater Form. 2008, suppl 1: 1071-1074.
7. Li, J.Z., Han, D., Liu, D.G., Wang, J.F., Zhang, N., Li, Z.H., 2014. A large vertical NC power spinning machine of 1000 kN. Form. Stamping Technol. 39, 1–5.
8. Yuan, S.J., Liu, W., Xu, Y.C., 2015. New development on technology and equipment of sheet hydroforming. J. Mech. Eng. 51, 20–28.
9. Cui, X.H., Yu, H.L., Wang, Q.S., 2018. Electromagnetic impulse calibration in V-shaped parts. Int. J. Adv. Manuf. Technol. 97, 2959–2968.
10. Cui, X.H., Zhang, Z.W., Yu, H.L., Xiao, X.T., Cheng, Y.Q., 2019. Springback calibration of a U-Shaped electromagnetic impulse forming process. Metals 9, 603.
11. Cui, X.H., Zhang, Z.W., Du, Z.H., Yu, H.L., Qiu, D.Y., Cheng, Y.Q., 2020. Inverse bending and springback-control using magnetic pulse forming. J. Mater. Process. Technol. 275, 116374.
12. Lai, Z.P., Cao, Q.L., Han, X.T., Liu, N., Li, X.X., Huang, Y.J., Chen, M., Cai, H., Wang, G.D., Liu, L.Y., Guo, W.Z., Chen, Q., Li, L. 2017. A comprehensive electromagnetic forming approach for large sheet metal forming. Procedia Eng 207:54–59.
13. Cui, X.H., Mo, J.H., Li, J.J., Zhao, J., Zhu, Y., Huang, L., Li, Z.W., Zhong, K., 2014. Electromagnetic incremental forming (EMIF): a novel aluminum alloy sheet and tube forming technology. J. Mater. Process. Technol. 214, 409–427.
14. Tan, J.Q., Zhan, M., Li, H.W. 2018. Dependence on forming parameters of an integral panel during the electromagnetic incremental forming process. Chinese Journal of Aeronautics. 31: 1625-1634.
15. Li, H.W., Yao, X., Yan, S.L., He, J., Zhan, M., Huang, L. Analysis of forming defects in electromagnetic incremental forming of a large-size thin-walled ellipsoid surface part of aluminum alloy. J. Mater.

Process. Technol. 2018, 255: 703-715.

16. Cui, X.H., Du, Z.H., Xiao, Ang., Yan, Z.Q., Qiu, D.Y., Yu, H.L., Chen, B.G. 2021. Electromagnetic partitioning forming and springback control in the fabrication of curved parts. J. Mater. Process. Technol. 288, 116889.
17. Cui, X.H., Mo, J.H., Li, J.J., Xiao, X.T., Zhou, B., Fang, J.X., 2016. Large-scale sheet deformation process by electromagnetic incremental forming combined with stretch forming. J. Mater. Process. Technol. 237, 139–154.

Figures

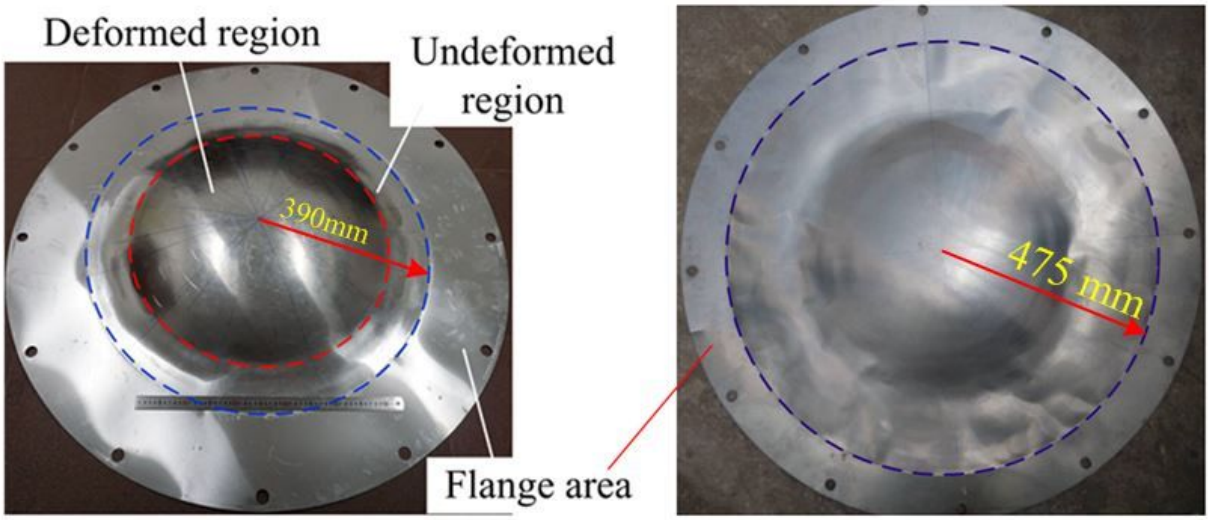

Figure 1

Deformation results using different blank holders sizes: (a) 390 mm radius blank holder (b) 475 mm radius blank holder

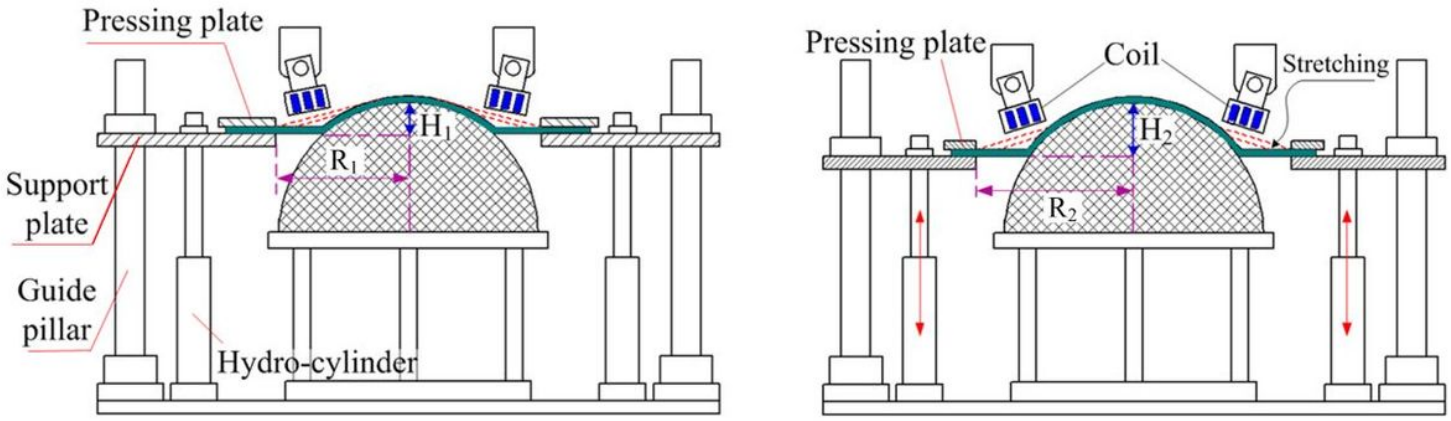

Figure 2

The forming principle with a variable blank holder structure: (a) blank holder radius R1 and a forming depth H1 and (b) blank holder radius R2 and a forming depth H2

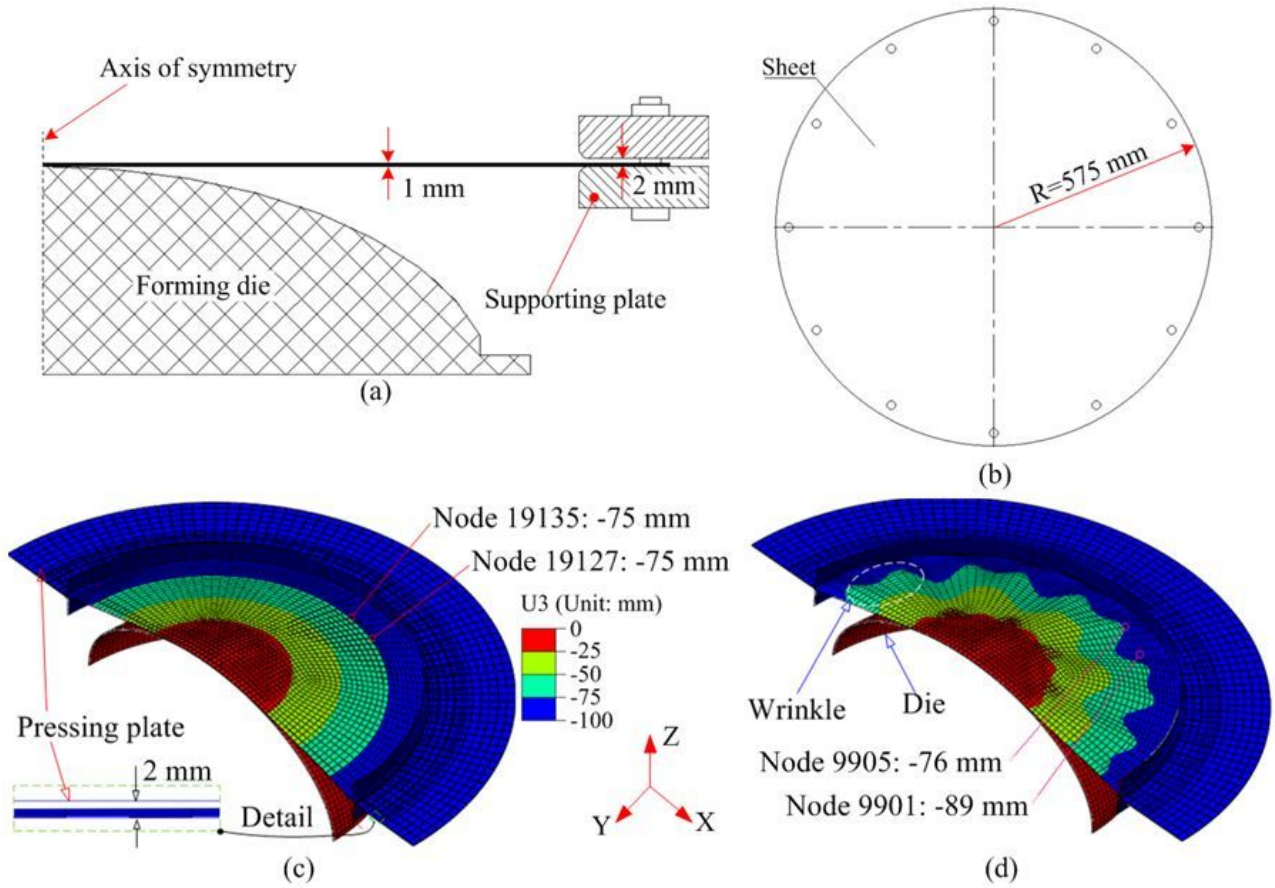

Figure 3

Sheet metal wrinkle simulation for 100 mm drawing depth: (a) forming system, (b) sheet metal, (c) sheet solid elements, and (d) sheet shell elements

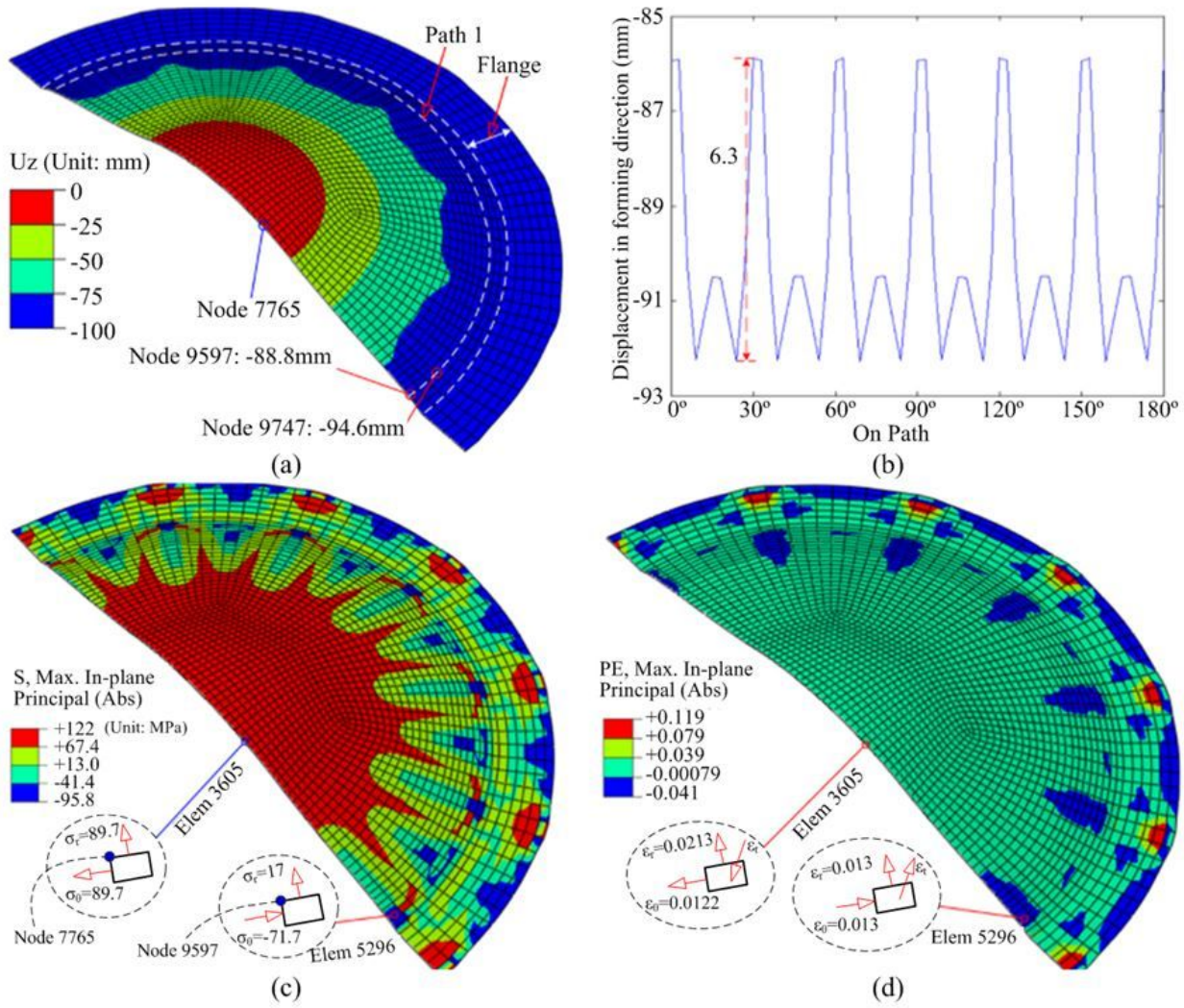

Figure 4

The deformation results for: (a) displacement, (b) Path 1 data, (c) stress, and (d) strain

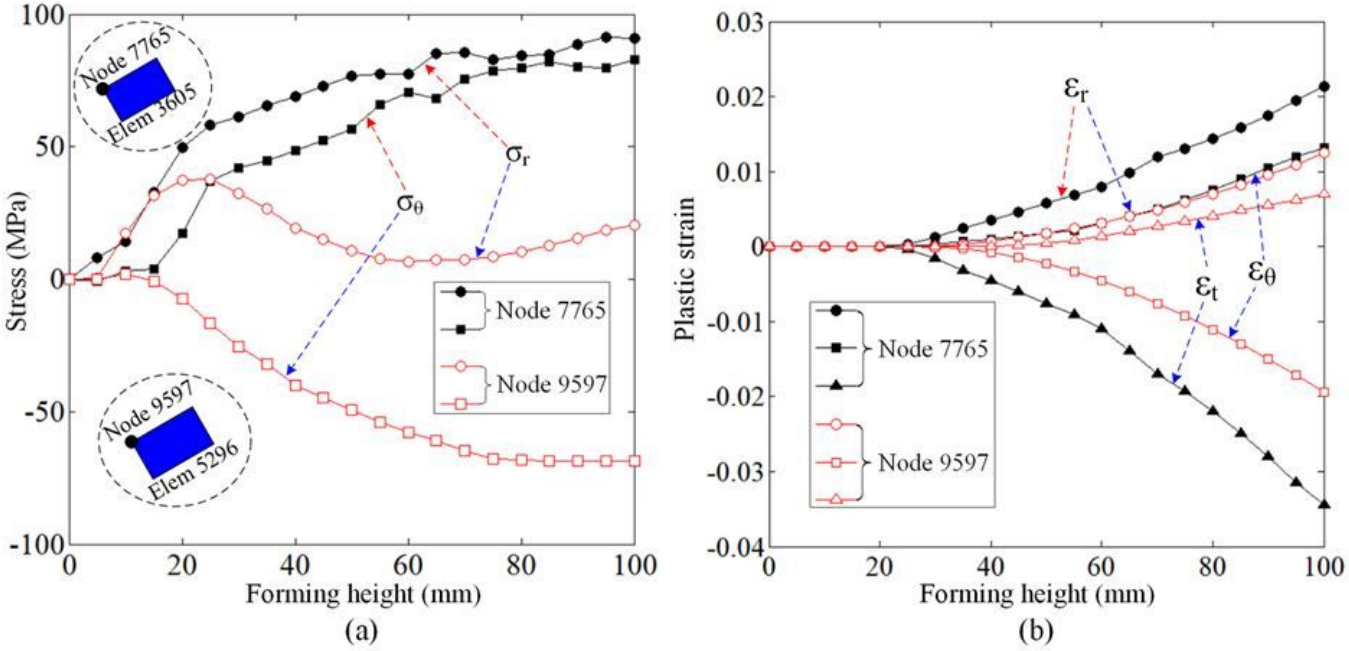

Figure 5

Changes in stress (a) and strain (b) depending on the forming height

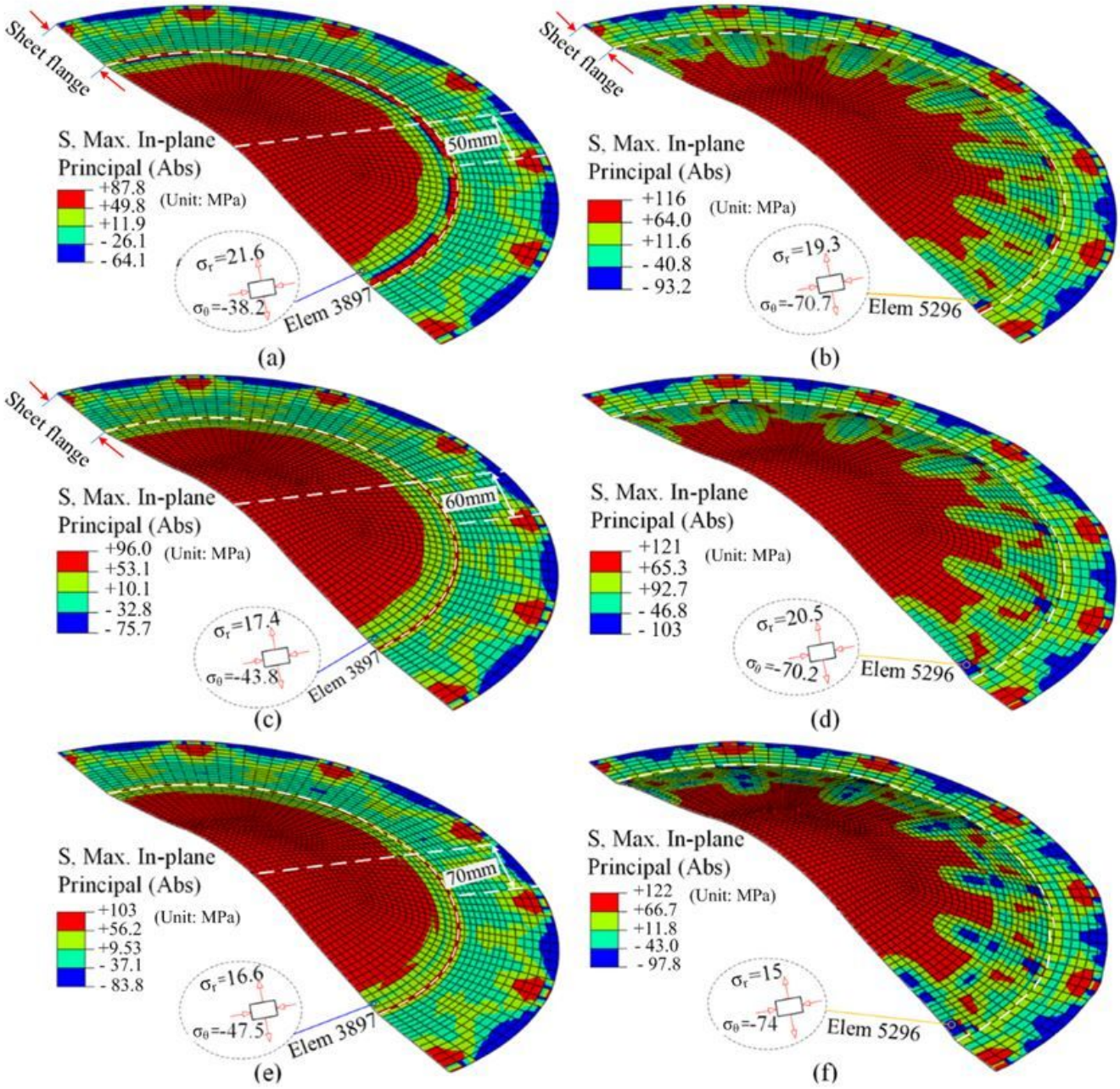

Figure 6

The stress distribution for various blank holder combinations: (a) and (b) Scheme 1, (c) and (d) Scheme 2, (e) and (f) Scheme 3. (a) H1 = 50 mm, (b) H2 = 100 mm, (c) H1 = 60 mm, (d) H2 = 100 mm, (e) H1 = 70 mm, (f) H2 = 100 mm

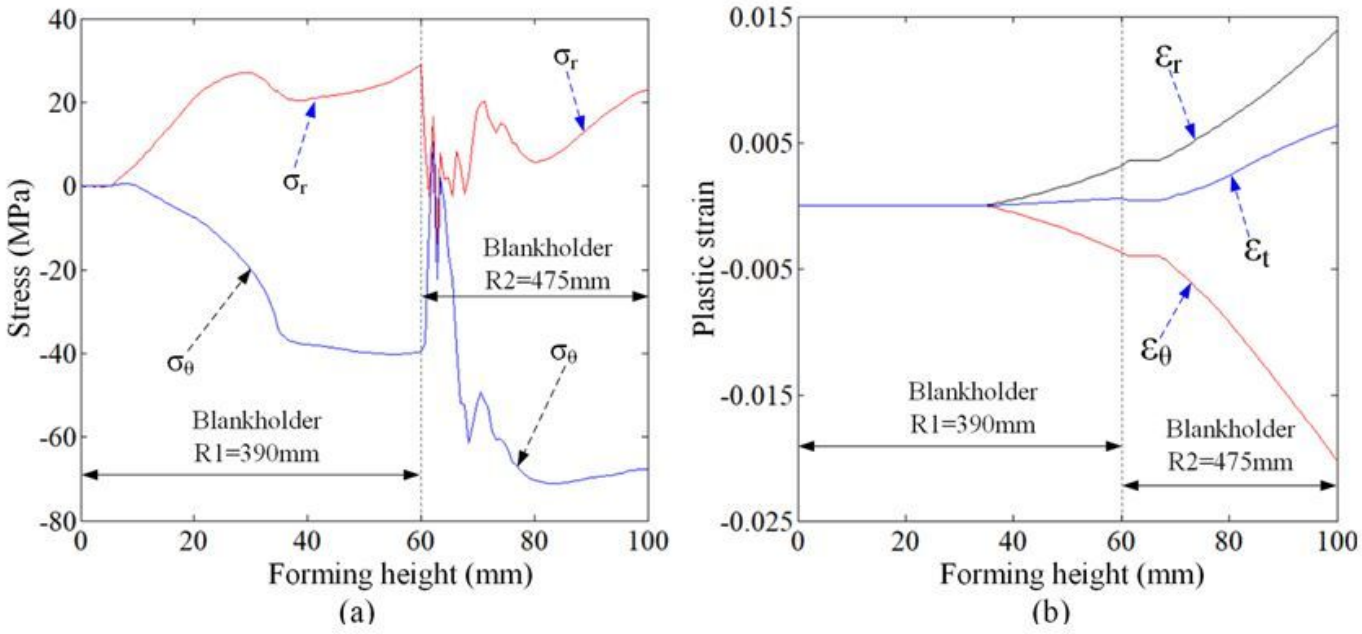

Figure 7

Changes in node 9597 stress (a) and strain (b) when observing Scheme 2

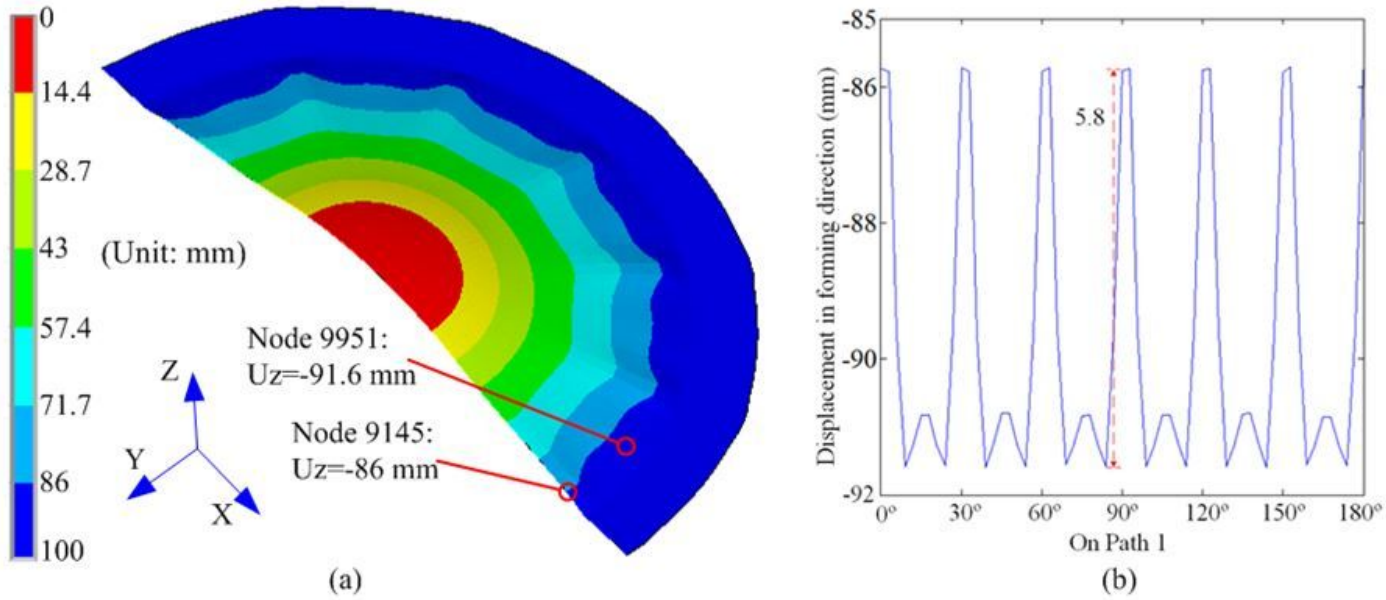

Figure 8

The deformations for two blank holder forming systems (a) displacement and wrinkle (b) Path 1 data

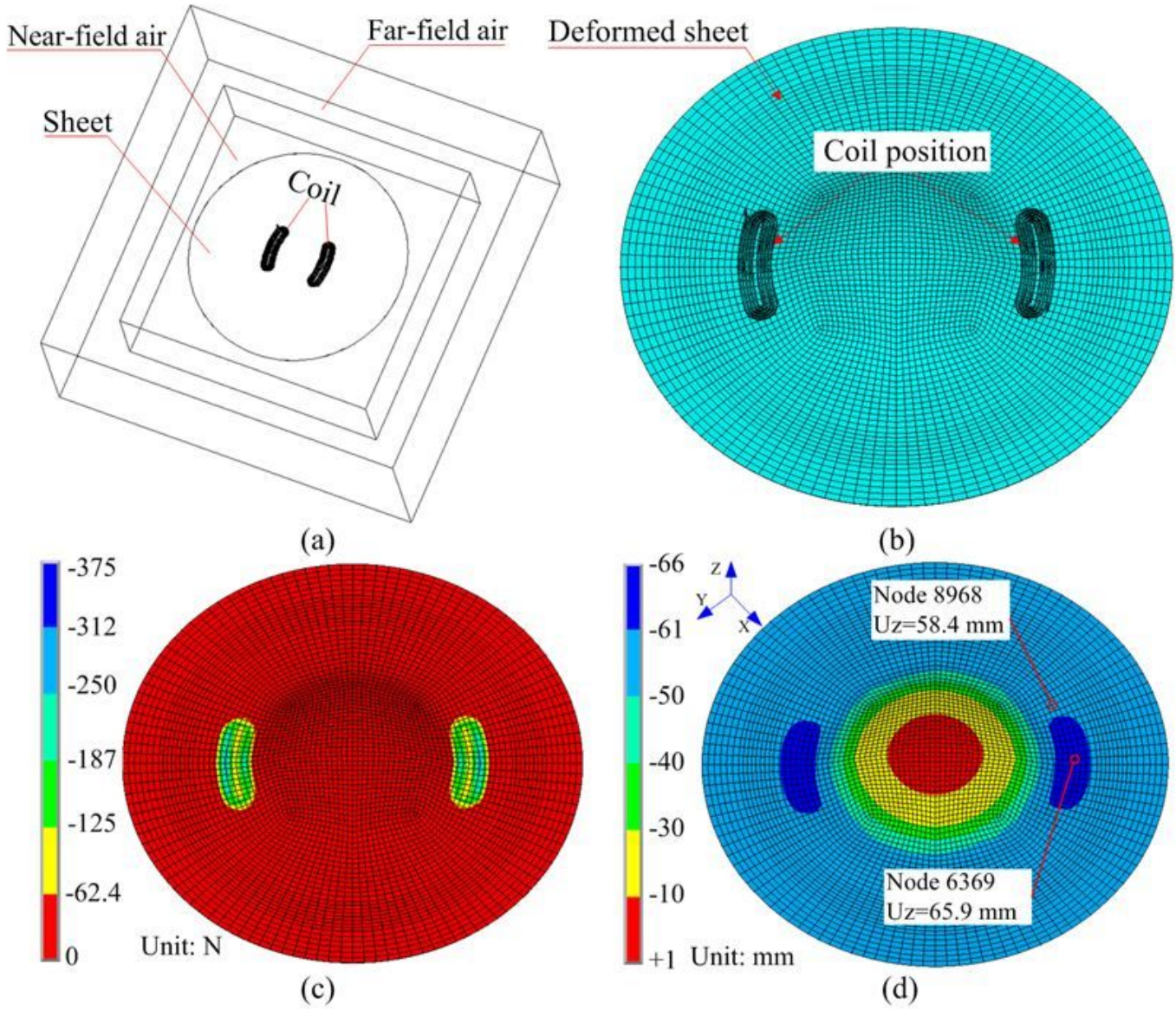

Figure 9

Finite element model; (a) electromagnetic model, (b) meshes, (c) magnetic force, and (d) sheet deformation results after the 19th discharge

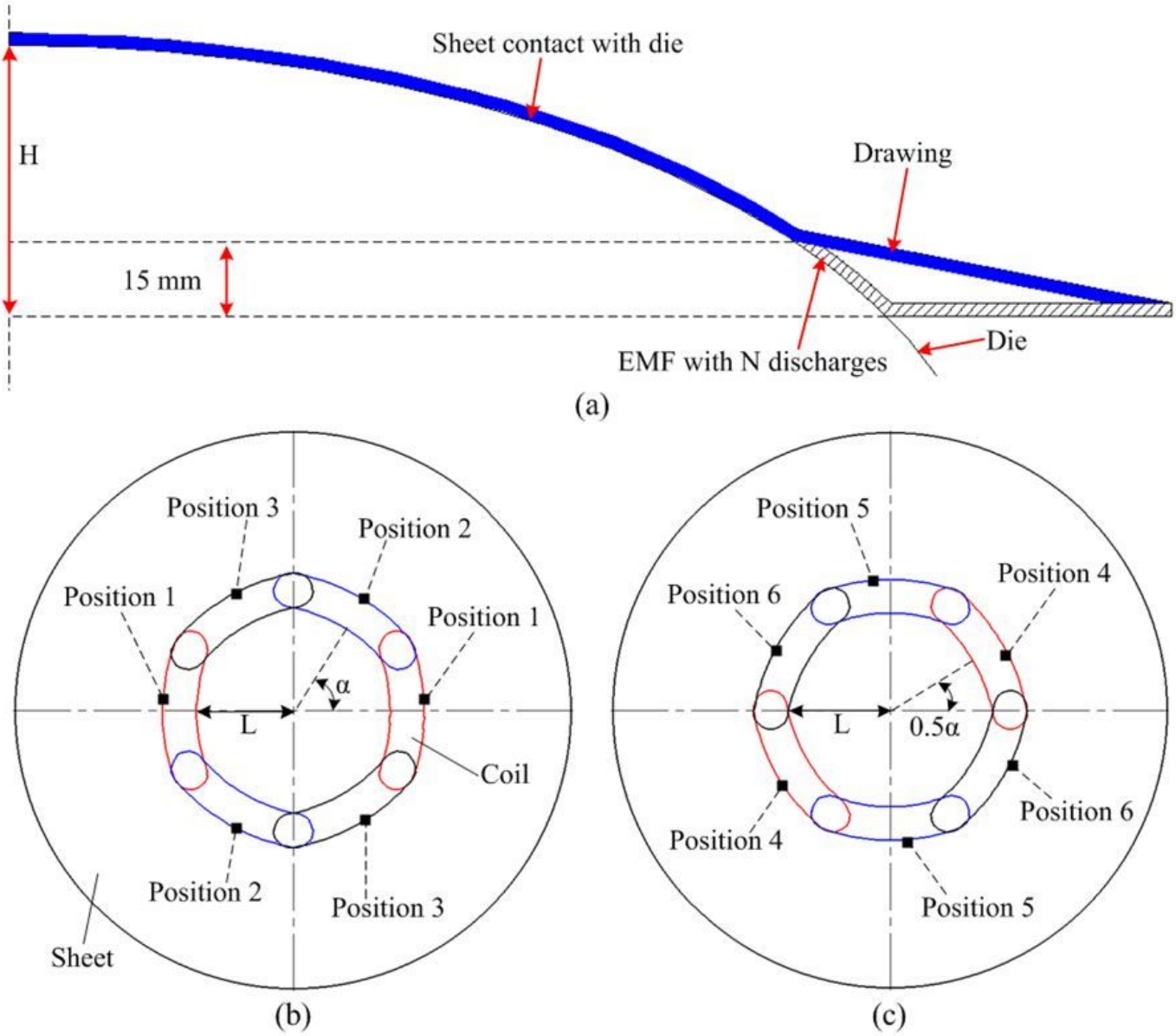

Figure 10

The EMIF process schematic diagram: (a) forming process in n-th layer, (b) discharge positions during the first turn, and (c) discharge positions during the second turn

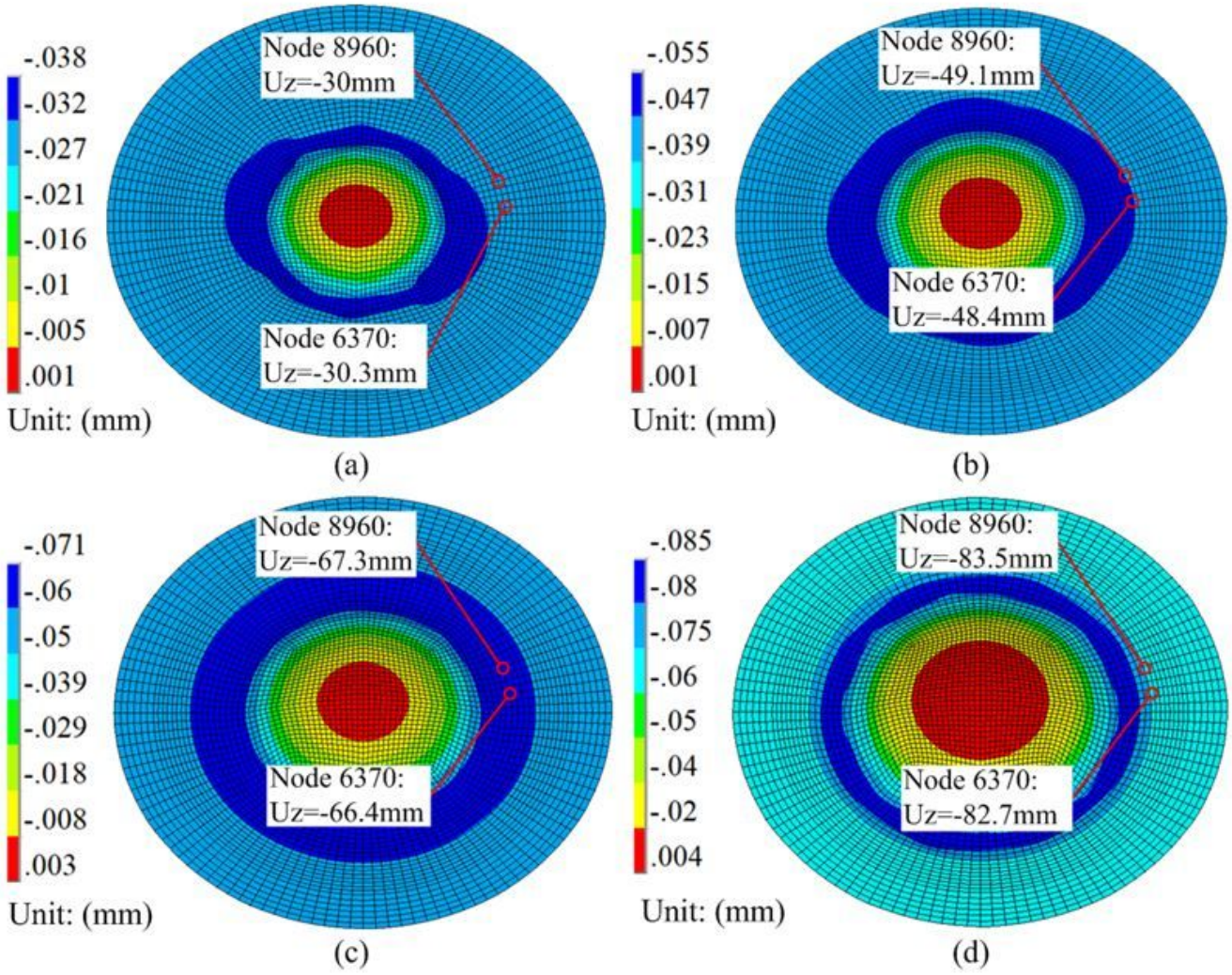

Figure 11

Deformed sheet shapes for various layers: (a) after 10th discharge, (b) after 18th discharge, (c) after 26th discharge, and (d) after 36th discharge

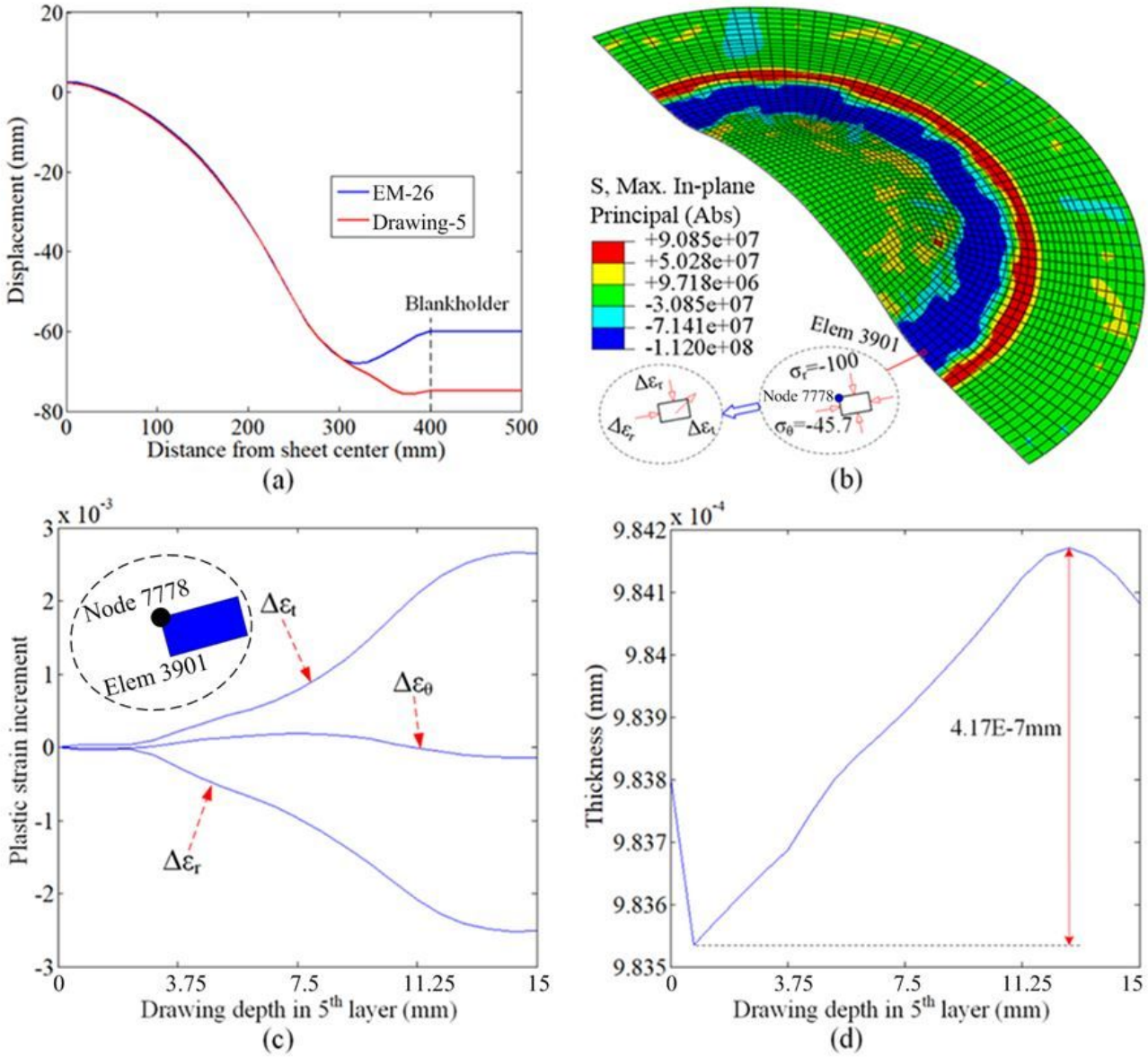

Figure 12

Deformation results after the 5th drawing: (a) deformation profiles, (b) the 3D stress distribution, (c) Node 7778 plastic strain increment during the 5th drawing, and (d) Node 7778 thickness changes during the 5th drawing

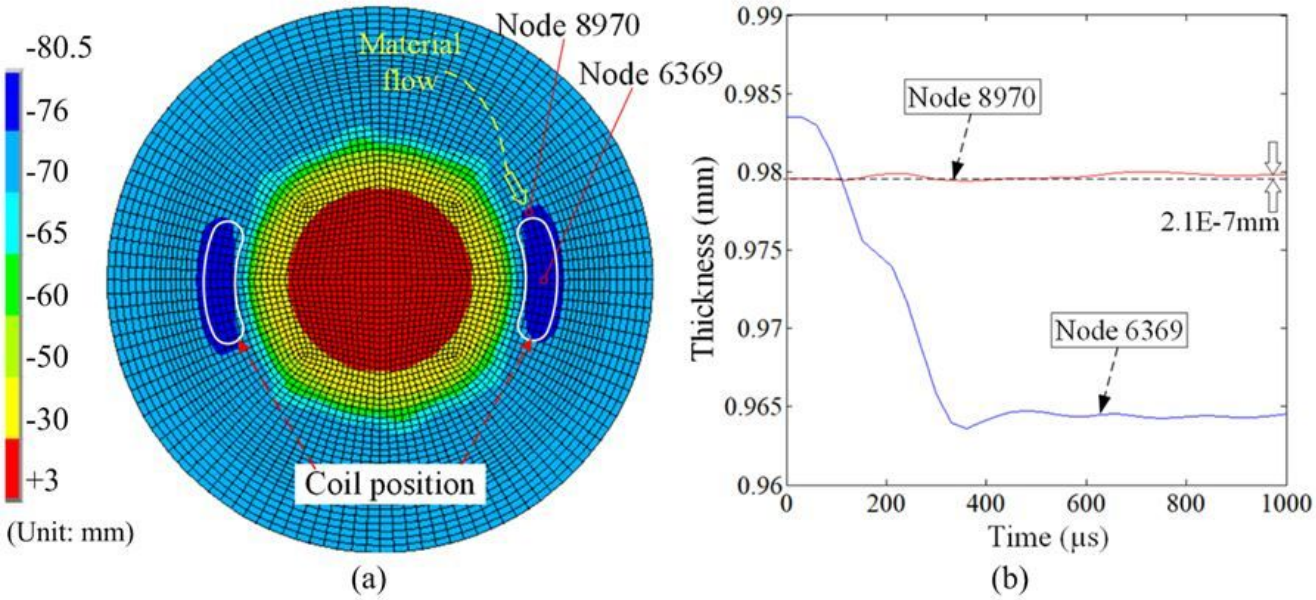

Figure 13

Results after the 27th coil discharge: (a) the 3D deformation shape and (b) changes in thickness (in time)

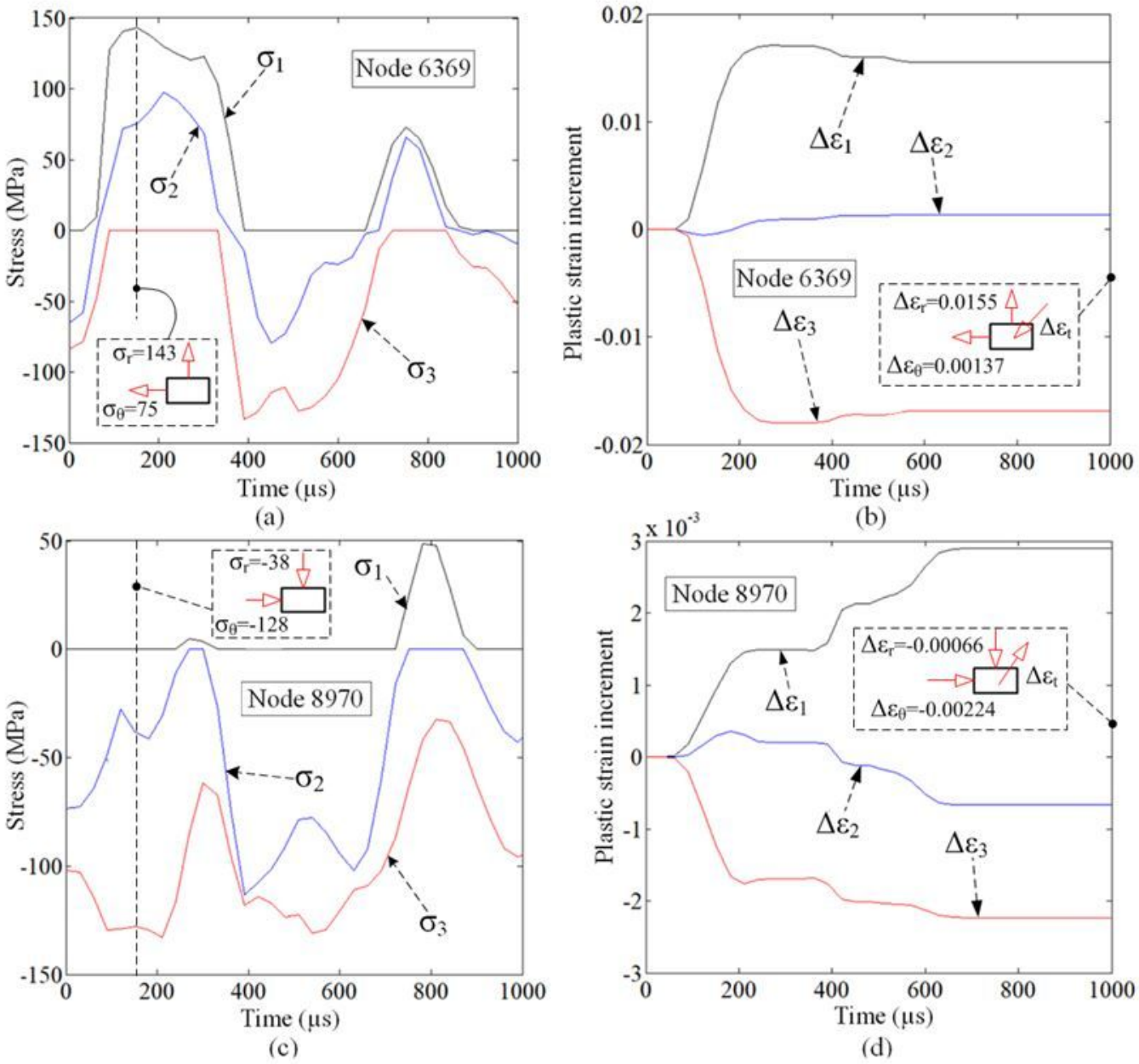

Figure 14

Changes in stress and strain with time during 27th discharge: (a) Node 6369 stress, (b) Node 6369 strain, (c) Node 8970 stress, and (d) Node 8970 strain

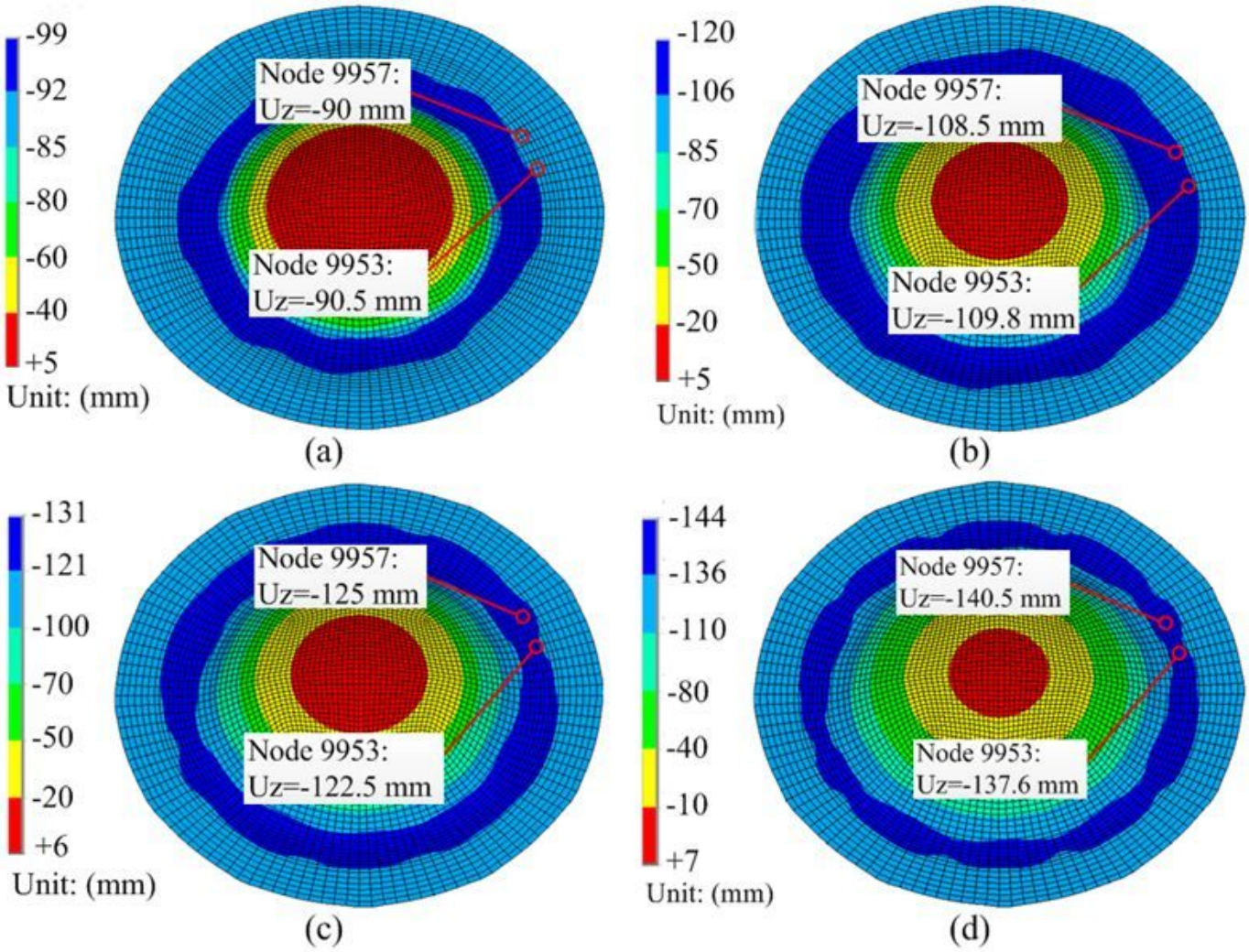

Figure 15

Deformed sheet shapes for different layers: (a) after the 46th discharge, (b) after the 56th discharge, (c) after the 66th discharge, and (d) after the 76th discharge

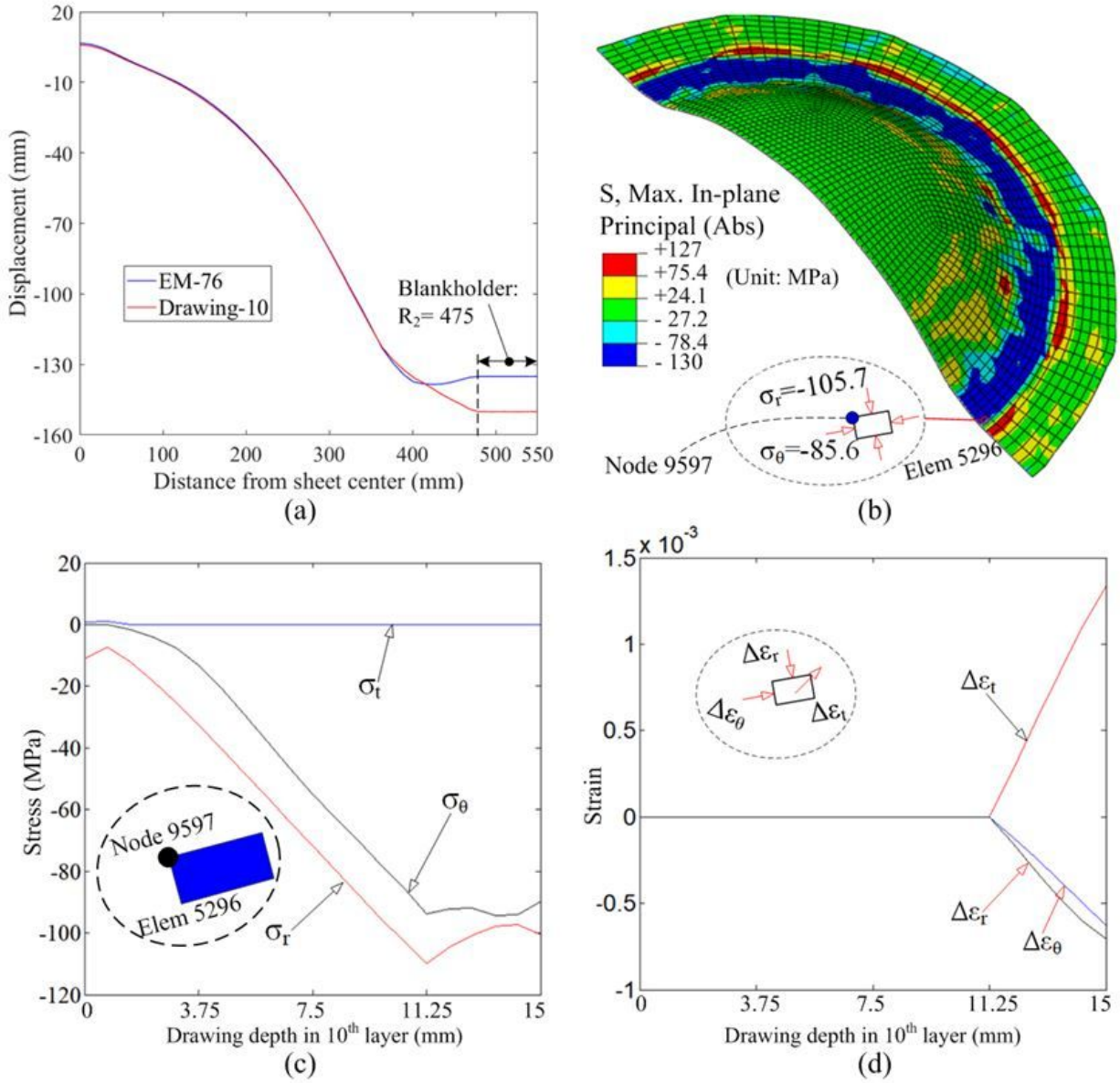

Figure 16

Deformation results after the 10th drawing: (a) the 2D deformed profiles, (b) the 3D stress distribution, (c) Node 9597 stress during the 10th drawing, and (d) Node 9597 strain variations during the 10th drawing

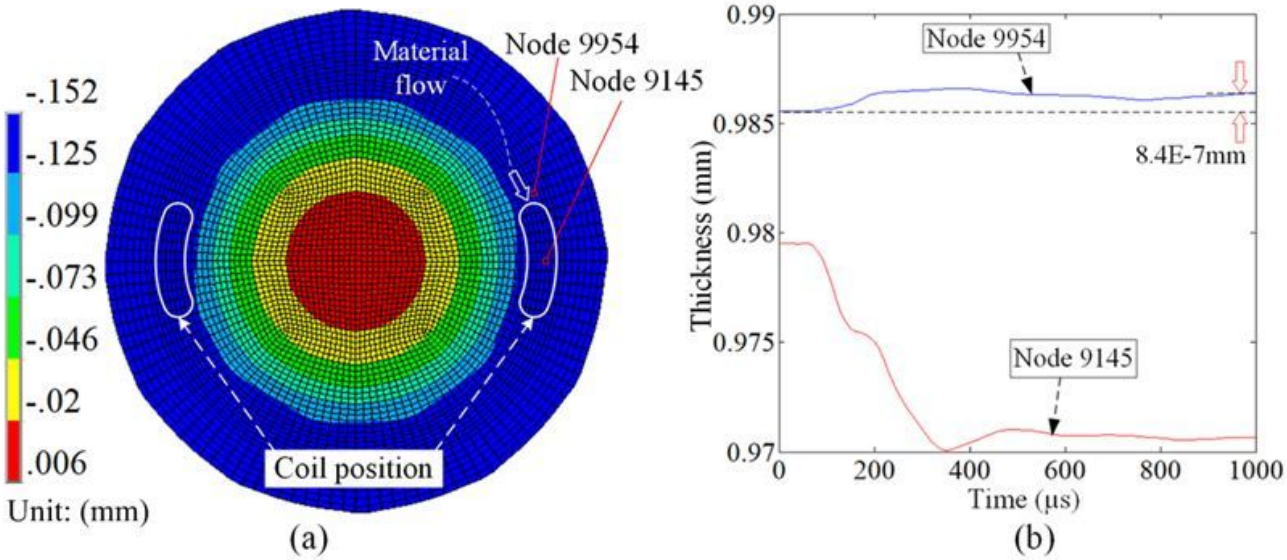

Figure 17

Results of the 77th coil discharge: (a) the 3D deformation shape and (b) variations in thickness

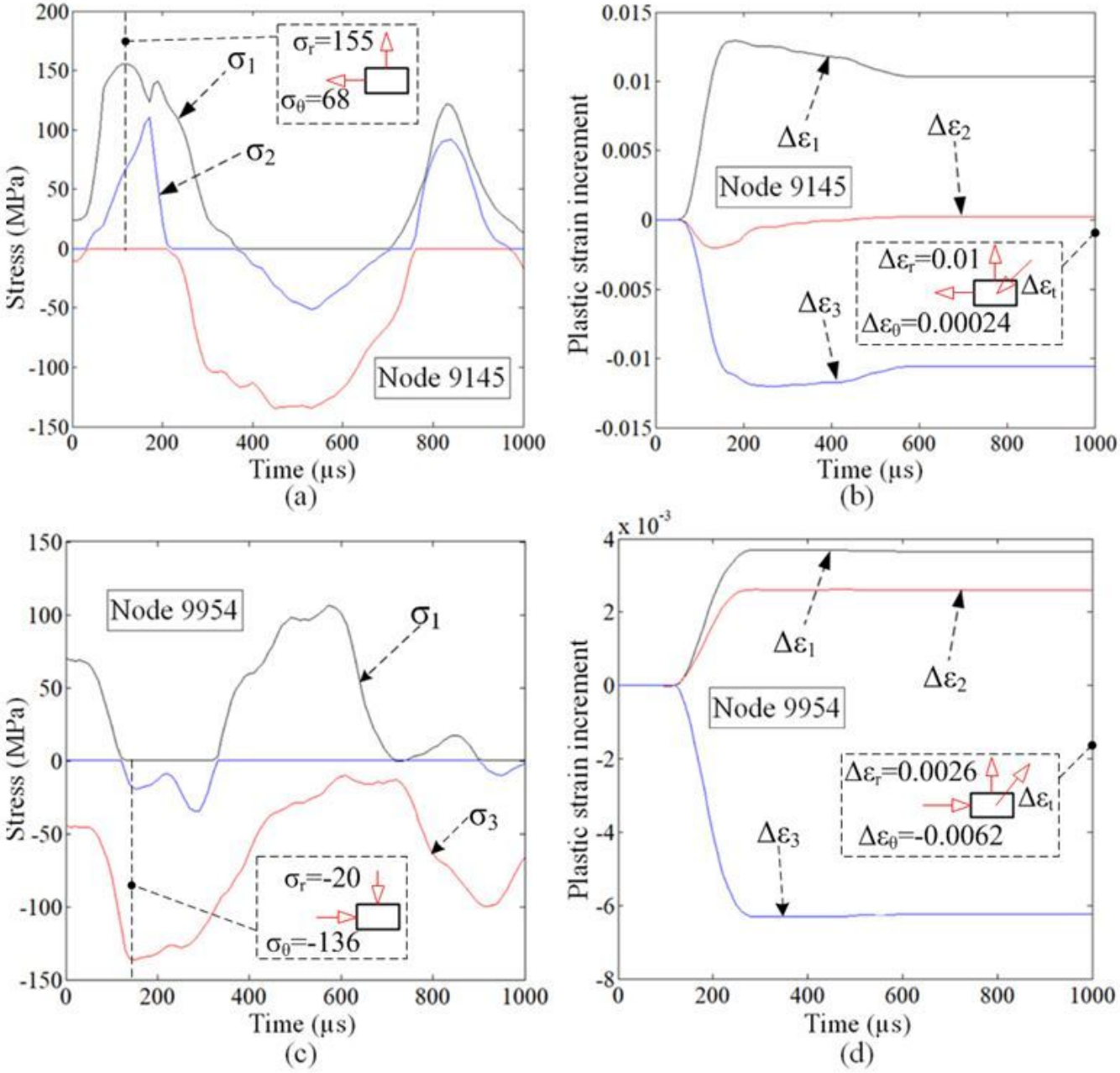

Figure 18

Changes in stress and strain depending on the time during the 77th discharge: (a) Node 9145 stress, (b) Node 9145 strain, (c) Node 9954 stress, and (d) Node 9954 strain

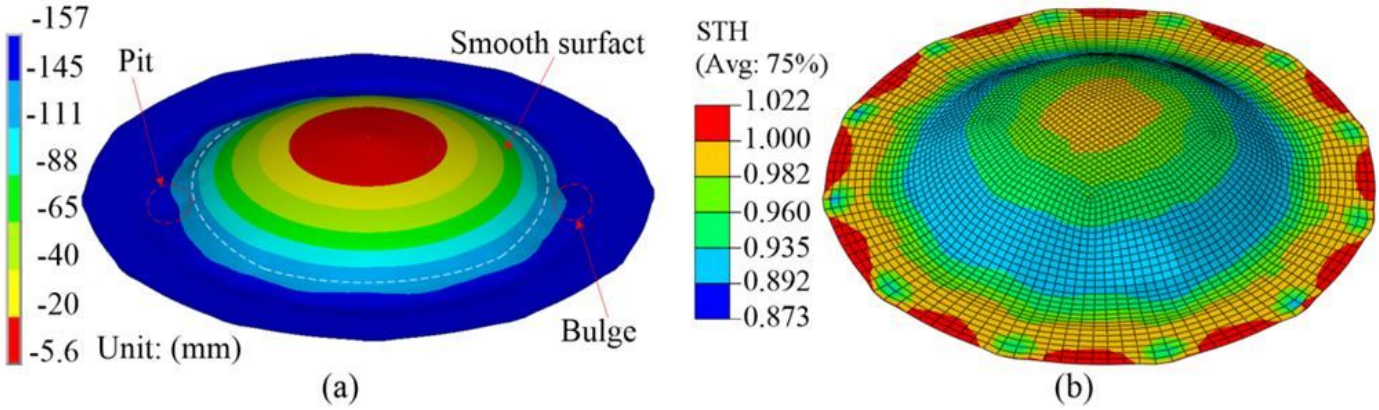

Figure 19

Final deformation results: (a) 3D deformation shape and (b) thichness

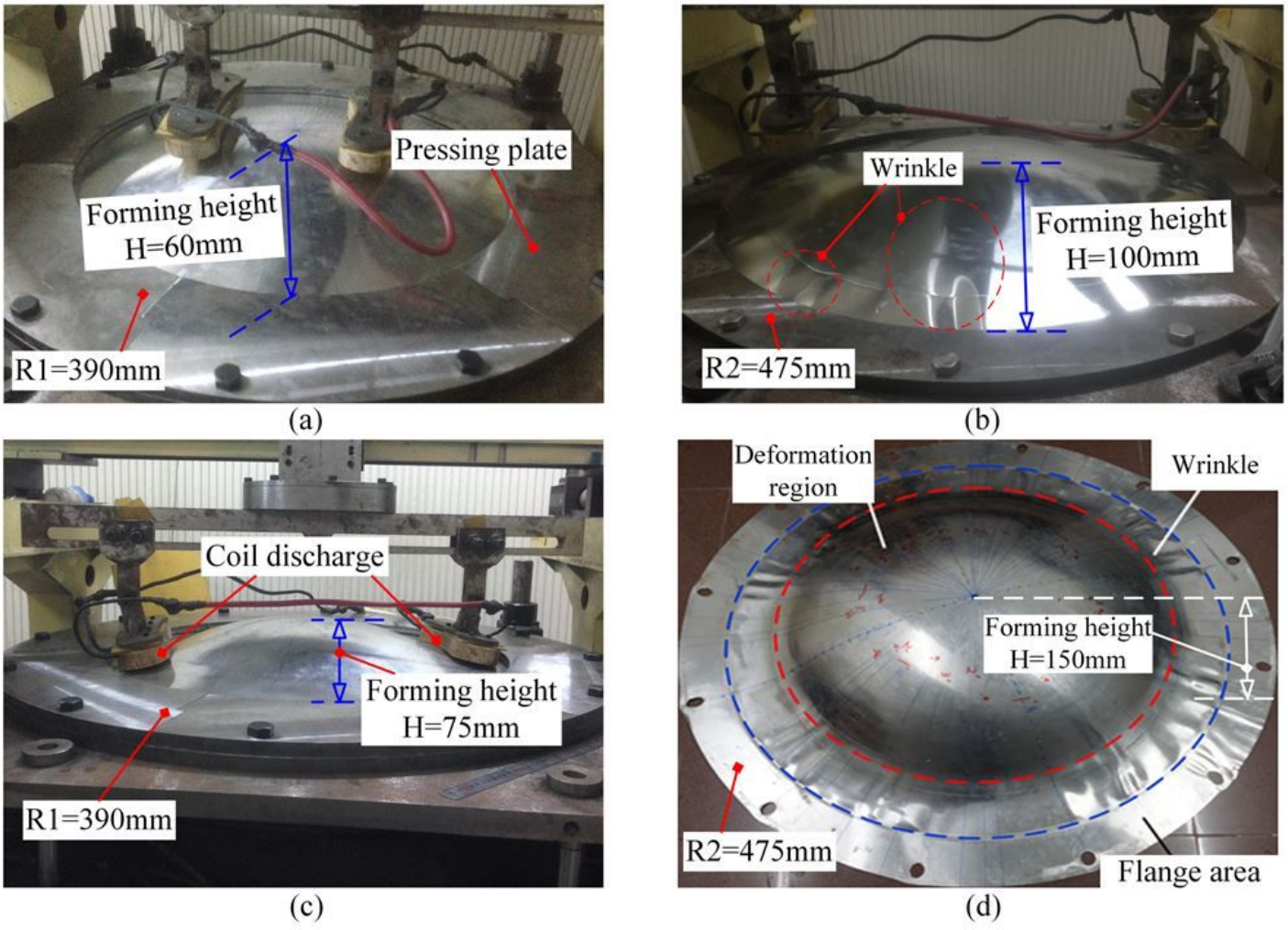

Figure 20

Experimental results: (a) quasi-static drawing with 390 mm blank holder and H1 = 60 mm, (b) quasi-static drawing with 475 mm blank holder and H2 = 100 mm, (c) electromagnetic forming with 390 mm blank

holder and H1 = 75 mm, and (d) electromagnetic forming with 475 mm blank holder and H2 = 150 mm

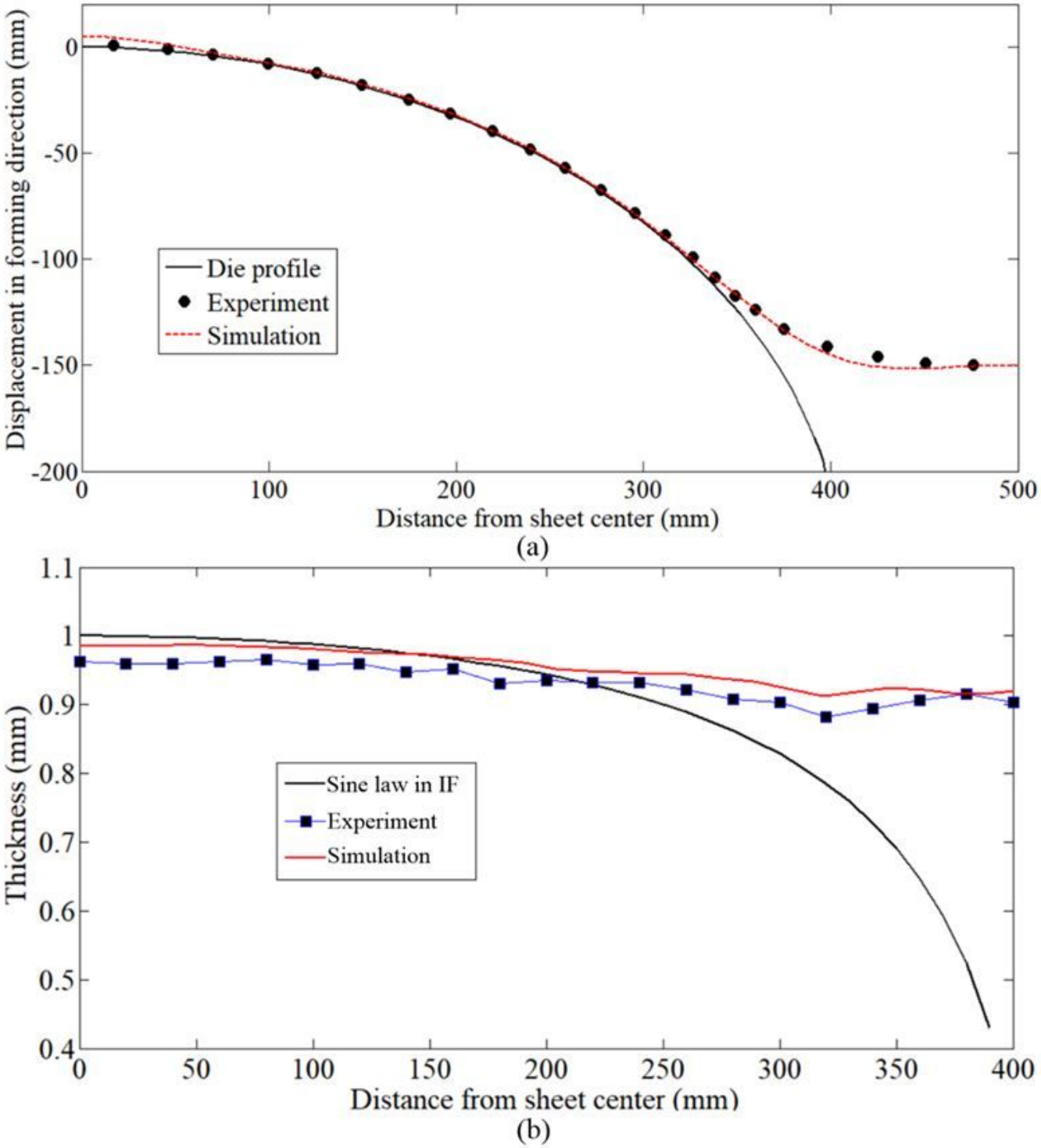

Figure 21

Comparison between the simulation and experimental results (a) sheet profiles (b) thickness